Available online at website: https://journal.bcrec.id/index.php/bcrec

Bulletin of Chemical Reaction Engineering & Catalysis, 19 (4) 2024, 585-598

Research Article

Heterobimetallic Zn^{2+}/Co^{2+} Monocarboxylates as Precursors for ZnO Microparticles Doped with Cobalt and its Photocatalytic Activity in Methyl Orange Oxidation

Hélder Inocêncio Ferreira Correa, Ralf Ricardo Ramalho Jr, Adhimar Flávio Oliveira, Fábio da Silva Lisboa*

Physics and Chemistry Institute of the Federal University of Itajubá (IFQ/UNIFEI), BPS Avenue, 1303, ZIP Code 37500-903, Itajubá-MG, Brazil.

Received: 19th September 2024; Revised: 1st November 2024; Accepted: 2nd November 2024
Available online: 10th November 2024; Published regularly: December 2024

Abstract

In this work, zinc oxide microparticles doped with cobalt were prepared from two novel layered heterobimetallic monocarboxylates as precursors to obtain uniform shape and size oxide particles, aiming for a photocatalytic removal of methyl orange. Both monocarboxylates produced ZnO doped with Co_2O_3 after calcination at 700 or 900 °C, in 7 or 12 hours. The particles formed by the laurate precursor presented rectangular prisms shaped, while those formed from stearate were sphere-like particles. All particles ranged from 0.1 to 0.9 µm size, with a direct bandgap of 2.2 to 2.6 eV and an indirect bandgap of 0.25 to 1.70 eV. The ZnO/Co prepared presented photocatalytic activity on methyl orange photodegradation. The solid prepared by the laurate precursor showed a photodegradation rate of 0.00185 min^{-1}, while the one obtained from the stearate precursor presented a photodegradation rate of 0.00860 min^{-1}, eight times greater. These results show that the material may be very useful in removing dyes from water samples.

Keywords: monocarboxylates; dye; zinc oxide; layered materials; degradation

How to Cite: Correa, H. I. F., Ramalho Jr, R. R., Oliveira, A. F., Lisboa, F. d. S. (2024). Heterobimetallic Zn2+/Co2+ Monocarboxylates as Precursors for ZnO Microparticles Doped with Cobalt and its Photocatalytic Activity in Methyl Orange Oxidation. *Bulletin of Chemical Reaction Engineering & Catalysis*, 19 (4), 585-598 (doi: 10.9767/bcrec.20211)

Permalink/DOI: https://doi.org/10.9767/bcrec.20211

Supporting Information (SI): https://journal.bcrec.id/index.php/bcrec/article/downloadSuppFile/20211/5332

1. Introduction

Most organic components found in drinking water systems come from wastewater originating from industries and agriculture, and many of them have been described as hazardous to the environment. Some examples of those are dyes and pesticides, respectively [1]. Dyes are widely used in many industries; their production per year is more than 7 tons, which generates a massive concern about their presence in the environment, especially in water, where they can remain for long periods, and there are a lot of drawbacks to removing it [2]. For example, methyl orange (MO) is an azo dye very employed in the food, paper, and textile industries; besides the economic importance of MO, this organic compound has high toxicity and has no easy biodegradability; therefore, robust methods are required for its total removal from drinking water [3,4]. Considering the three types of treatment for wastewater, biological degradation, physical separation, and chemical process [2], the last one can promote the chemical decomposition of dyes by using heterogeneous photocatalysts, and this method has earned a considerable highlight nowadays [5].

Solids with semiconductor behavior have been intensively prepared and studied as heterogeneous photocatalysts. Generally, these solids have metal ions, like Ti^{4+}, Zn^{2+}, Co^{2+}, etc., in

* Corresponding Author.
Email: fabiolisboa@unifei.edu.br (F. S. Lisboa)

their composition. Kaur *et al.* prepared nano powders of ZnO from an organic precursor of oxalate by decomposition method [3]. The authors found that the material was active in pH 9 under UV irradiation, with degradation varying from 58.92 to 95.29% when the catalyst loading was raised because the increased active sites generated more hydroxyl radicals. Sha *et al.* worked with cobalt (Co) nanoparticles, and they obtained a rate constant equal to 2.444 min^{-1}, exemplifying the high activity of the material in MO degradation [5]. Peerakiatkhajohn *et al.* doped the ZnO with Al, reducing the oxide band gap and promoting the MO degradation under visible light irradiation [4]. These three works summarize the proposal to obtain a material mainly composed of a semiconductor to be applied in dye photodegradation. For this reason, ZnO particles doped with Co^{2+} with controlled dimensions, sizes, and morphology, could have an interesting photocatalytic activity. This material could be synthesized by a precursor, such as a layered metal monocarboxylate with ions zinc and cobalt, because this material class has many applications, including acting as a template for mixed oxides synthesis [6].

Layered metal monocarboxylates are commonly built by neutral layers of organic chains in *all-trans* conformation, and the carboxylate groups are coordinated in bridge-bidentate mode at the metallic centers [7]. They can be important in oil painting degradation studies, corrosion inhibitors, and as precursors of nanostructured oxides [8-10]. Mainly, obtaining oxides with specific and well-defined sizes and morphology is very important to enhance their catalytic, electrical, optical, and magnetic properties [11-13]. For example, Saravanan *et al.* prepared ZnO by different methods using zinc acetate as a precursor and tested all products in photocatalytic degradation of dyes. They observed that the crystallite size directly affected the surface area and, consequently, the activity of these materials [14]. Sun *et al.* synthesized Co_3O_4 nanoparticles using a template precursor, obtained particles with high surface area and tested this material for CO oxidation. The catalysis of this material with uniform size and shape presented a conversion rate near 100% [15]. Thus, ZnO can have its band gap shifted to higher or lower energies with transition metal ions like Cu, Co, or Ni, and thus, its photocatalytic behavior is enhanced [16-19].

Therefore, using metal monocarboxylates as oxide precursors can contribute to obtaining controlled particles of metal transition oxides; for that, the strategy can be using heavy metal carboxylates. So, different monocarboxylates can be prepared by combining metallic ions such as Mn^{2+}, Fe^{2+}, Co^{2+}, Ni^{2+}, Cu^{2+}, and Zn^{2+} with long-chain carboxylic acids, like lauric and stearic acids [20,21]. Also, it is possible to synthesize monocarboxylates with two different ions, originating a heterometallic monocarboxylate [22].

In this work, we proposed the synthesis of two novel heteronuclear monocarboxylates with the metallic ions Zn^{2+} and Co^{2+} and their use to obtain oxides with controlled size and shape, using the monocarboxylates derivative from the acids lauric and stearic. Also, the mixed oxides generated in this study were applied to methyl orange dye oxidation to test its photocatalytic behavior.

2. Materials and Methods

2.1. Chemicals

All reactants used in this work were commercially obtained and employed without further purification. The chemicals used to the synthesis and photodegradation studies were: lauric acid (Aldrich, 98%), stearic acid (Aldrich, 98%), ethanol (VETEC, 99.5%), NaOH (Dinâmica, 98%), distilled water, zinc chloride hexahydrate (Cromoline, 98%), Cobalt(II) chloride hexahydrate (Cromoline, 98%) and methyl orange (Dinâmica P.A.).

2.2 Synthesis of the Monocarboxylates of Zinc and Cobalt Laurate (ZnCoL) and Zinc and Cobalt Stearate (ZnCoS)

The synthesis of the two novel monocarboxylates, laurate and stearate of Zn^{2+} and Co^{2+}, followed the same steps and quantities for both compounds and was based on the synthesis described by Lisboa *et al.* with few modifications [21]. The first step consisted of preparing the monocarboxylate salt of sodium (sodium laurate/sodium stearate) and for that, 3.46×10^{-2} mol of lauric acid or stearic acid was completely dissolved in 20 mL of ethanol at 40 °C under magnetic stirring (800 rpm). Then, to neutralize the acid solution previously prepared (under heating and magnetic stirring), 3.46×10^{-2} mol of NaOH was added. To this system, 50 mL of distilled water was added until the neutralization reaction completely dissolved the white solid. The second step was the addition of the metallic salts to the solution to form Zn^{2+} and Co^{2+} laurate and stearate. For that, a solution prepared with 1.15×10^{-2} mol of $ZnCl_2.6H_2O$ and 0.58×10^{-2} mol of $CoCl_2.6H_2O$ in 50 mL of distilled water was added slowly (30 drops per minute), to the sodium monocarboxylate solution, under heating and magnetic stirring (40 °C and 800 rpm). After the complete addition of the salt solution, the heating was cessed, and the system was maintained under magnetic stirring (800 rpm) for 2 hours. The purple solids obtained were washed with acetone 10 times, followed by washing with distilled water 2 times, and dried at 60 °C for 48 hours.

2.3. Synthesis of the ZnO Particles Doped with Cobalt

The ZnO particles were obtained by calcination of the monocarboxylates in a muffle oven (EDG F-3000 10 P) at 700 and 900 °C for 7 and 12 hours. The calcination procedure was made by a heating curve with 1.0 g of each sample accommodated in alumina crucibles, from room temperature (about 30 °C) to 150 °C at a rate of 5 °C per minute, keeping at 150 °C for 30 minutes and then increasing it 5 °C per minute until the desired final temperature (700 or 900 °C) and time (7 or 12 hours).

2.4. Characterization and Equipment

The FTIR-ATR (Fourier Transform Infrared Spectroscopy with attenuated total reflectance) spectra were recorded in a Perkin Elmer Spectrum 100 instrument, equipped with a diamond crystal ATR module, in the range of 650-4000 cm^{-1}, resolution of 4 cm^{-1} and 16 scans. The X-ray diffractograms were obtained in a Malvern Panalytical X'Pert PRO equipped with cooper target (k_α = 1.5404 Å) at the following conditions: current of 30 mA, voltage of 40 kV, step of 0.02°, time per step of 0.5 seconds, and scan range from 3 to 70° of 2θ degrees. Thermogravimetric analyses (TGA) were made in a Mettler Toledo equipment, model TG 50, with oxygen flow (50 $mL.min^{-1}$) from 30 to 1000 °C and a heating rate of 10 $°C.minute^{-1}$. The scanning electron microscope (SEM) images were obtained in a MIRA-3 FEG-SEM Tescan microscope. The grain sizes were determined by analyzing SEM images using ImageJ software. The diffuse reflectance of UV-Vis measurements was carried out using a BLACK-COMET-SR spectrometer from 200 to 1080 nm, equipped with a Sl1 halogen light source visible and NIR emitting lengths between 350 and 2500 nm, and DP-400-UVVIS-SR optical fiber for reflectance measurements. To estimate the samples' direct and indirect optical bandgap (Eg) transitions, we employ the Kubelka-Munk (KM) method in combination with the Tauc plot. This method is based on Equation (1), as applied in studies by Azab *et al.*, Toledo *et al.*, and Patel *et al.* [23-25].

$$F(R) \equiv \frac{(1-R)^2}{2R} = \frac{K}{S} = \frac{B\left(h\nu - E_g\right)^n}{h\nu} \quad (1)$$

where, K and S are the coefficients of absorption and scattering, h is the Planck constant, ν is the frequency, and n describes the type of electronic transition between energy levels.

2.5. Photodegradation of Methyl Orange (MO)

The photodegradation experiments were conducted in a dark chamber containing a lamp with visible light irradiation (60 W; 12 V). The spectra were collected in a Kasvi spectrophotometer, model K-37, in a range of 190 to 600 nm, at 35 °C, every 15 minutes. Initially, a pre-concentration time of 30 minutes was conceived because of the possible adsorption of MO on the solid surface. In this stage, the irradiation lamp was turned off. So, after this period, the lamp was turned on, and the photodegradation experiments started. The procedure consisted of using 7.5 mL of a solution of methyl orange in an initial concentration of 1.0×10^{-3} $mol.L^{-1}$ in the presence of 13 mg of the photocatalysts, ZnO/Co calcinated at 700 °C for 12 hours. The systems remained in magnetic agitation (800 rpm) at intervals of 15 minutes, and spectra were collected after the total solid sedimentation by centrifugation at 3000 rpm. A control experiment was conducted to verify the photodegradation of the MO promoted only by the irradiation of the visible light, at the same conditions, except that the photocatalyst was not present in this experiment.

3. Results and Discussion

3.1 Characterization of Zinc Cobalt Laurate (ZnCoL) and Zinc Cobalt Stearate (ZnCoS)

The X-ray data of the synthesized monocarboxylates showed an expected profile of a layered material, in which it is possible to observe the basal planes in a range of 3 until 20° of 2θ, as seen in Figure 1. Black line for laurate of Zn^{2+} and Co^{2+} (ZnCoL) and red line for stearate of Zn^{2+} and Co^{2+} (ZnCoS). The basal spacing observed for each compound was 30.55 Å and 42.24 Å, respectively, which means that the layered structure for both materials consisted of double layers of the organic moiety coordinated to the metal ions centers [8,21,26].

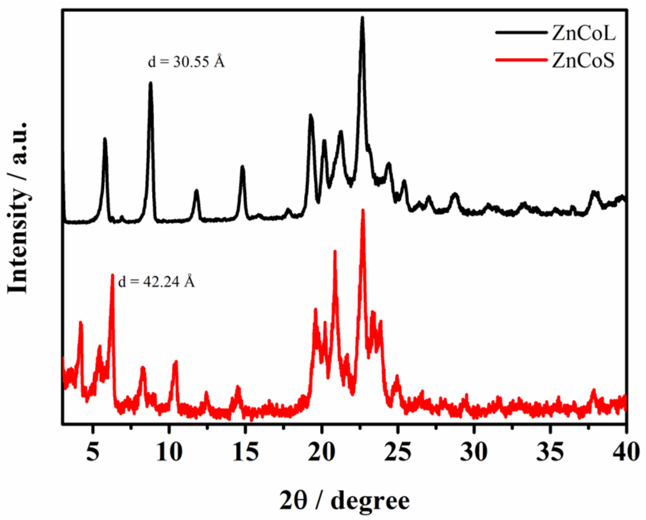

Figure 1. Diffraction profiles of the synthesized monocarboxylates of Zn^{2+} and Co^{2+}: ZnCoL (black line) and ZnCoS (red line).

Both compounds' FTIR spectra (Figure 2) presented the characteristic bands expected for monocarboxylates coordinated with metallic ions. It is possible to observe the main bands for each monocarboxylate, that can be assigned to the groups: CH of methyl and methylene groups in the region 2850 to 2950 cm^{-1}; the asymmetric and symmetric modes for COO^-, around 1590 and 1390 cm^{-1}, respectively; the progression bands (PB) in the region of 1300 cm^{-1} and the rocking mode of CH_2 in 720 cm^{-1}. These last two groups, PB and ρCH_2, denote that the organic chains are in *all-trans* conformation, and the values observed for the difference between the asymmetric and symmetric stretching of the carboxylate groups, $\Delta\upsilon \approx 120 - 140$ cm^{-1}, suggest a bridge bidentate coordination mode of the COO^{-1} to the metallic centers [7,8,27,28]. So, the layered structures are formed by double layers of organic chains in *all-trans* conformation, linked by the carboxylic groups coordinated to the metallic centers. Table 1 presents the resume of bands observed for each spectrum.

The SEM analysis showed plate-like morphology, with irregular edges, as seen in the micrographs in Figure 3. For the compound ZnCoL, the plates presented particles of about 3 times lower sizes than those presented for ZnCoS. The morphology was similar to those obtained by Gnen *et al.* [29]. Therefore, the XRPD, FTIR, and SEM results confirmed the formation of the laurate and stearate of Zn^{2+} and Co^{2+} ions.

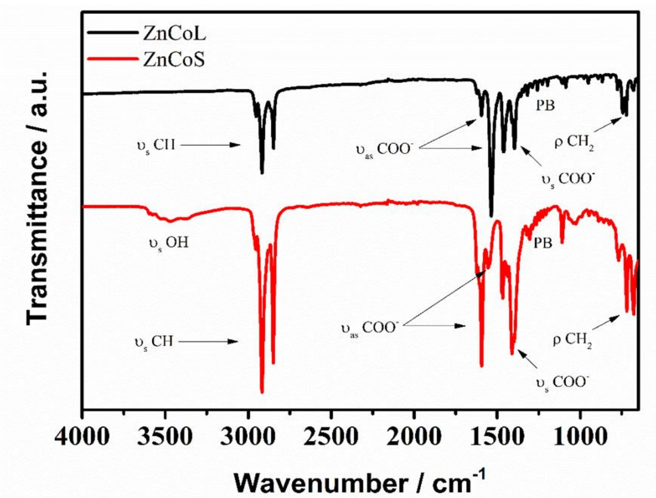

Figure 2. FTIR spectra obtained for the monocarboxylates of Zn^{2+} and Co^{2+}: ZnCoL (black line) and ZnCoS (red line).

3.2 Characterization of the ZnO Doped with Co^{2+} (ZnO/Co) Obtained from the Precursors: Zinc Cobalt Laurate (ZnCoL) and Zinc Cobalt Stearate (ZnCoS)

The products obtained after the calcination of the monocarboxylates precursors at 700 and 900 °C in 7 and 12 hours, did not present the phases of ZnCoL or ZnCoS, as seen in Figure 4. In Figures

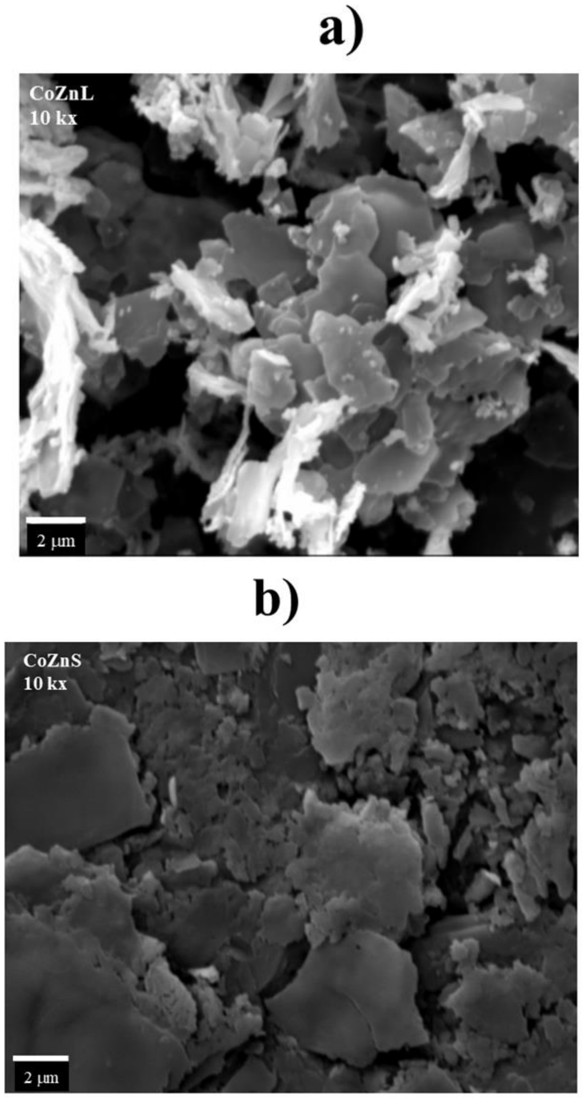

Figure 3. Micrographs of the synthesized monocarboxylates: a) ZnCoL and b) ZnCoS. Magnification of 10.000x for each compound.

Table 1. Vibrational modes (cm^{-1}) observed in the spectra of the monocarboxylates synthesized.

Monocarboxylate	OH	CH	COO^-	PB	CH_2	$\Delta\upsilon$
ZnCoL	-	2917 / 2849	1536 (as) 1397 (s)	1197 - 1320	722	125
ZnCoS	3460	2919 / 2850	1555 (as) 1411 (s)	1200 - 1330	720	144

4a and 4b, it is presented ZnCoL and ZnCoS, respectively, converted in ZnO (ICDD card No. 4-5-4711) due to peaks in the region between 30 and 70° of 2θ, characteristic of wurtzite, assigned with an asterisk (*) [29]. Also, the diffractograms showed the presence of CoO (ICDD card No. 98-002-8506), as can be observed by the peak near 40° (2 θ), which refers to the plane (311) assigned by a (♦) [15,30-32]. In Figure 4a (black line), it is also possible to observe a phase attributed to the presence of a layered double hydroxy salt $Zn_2Co_3(OH)_{10}2H_2O$ (JCPDS 21-1477) [31].

The micrographs obtained by SEM for the ZnO/Co synthesized from the precursors ZnCoL and ZnCoS are shown in Figures 5 and 6. The EDX analysis for all solids presented a Zn:Co ratio near 9.3, and the elementary maps showed good distribution for zinc, cobalt, and oxygen for all samples (see Supporting Information, Figures S1 and S2, respectively). Figure 5 shows that the morphology changed from plaques (see Figure 3) to quasi-rectangular prisms for the ZnO/Co calcinated at 700 °C in 7 or 12 hours (Figure 5a). In Figure 5b, the images obtained with a magnification of 100kx for the ZnO/Co calcinated at 900 °C for 7 hours, showed that the morphology was concentric plaques.

In Figure 6, the morphology of the calcination products of ZnCoS were more similar to irregular spheres than those formed by ZnCoL. We believe that the formation of oxide particles must pass a decomposition route, creating a reverse micellar phase of monocarboxylates, as reported in the literature [33,34]. Thus, the formation of the

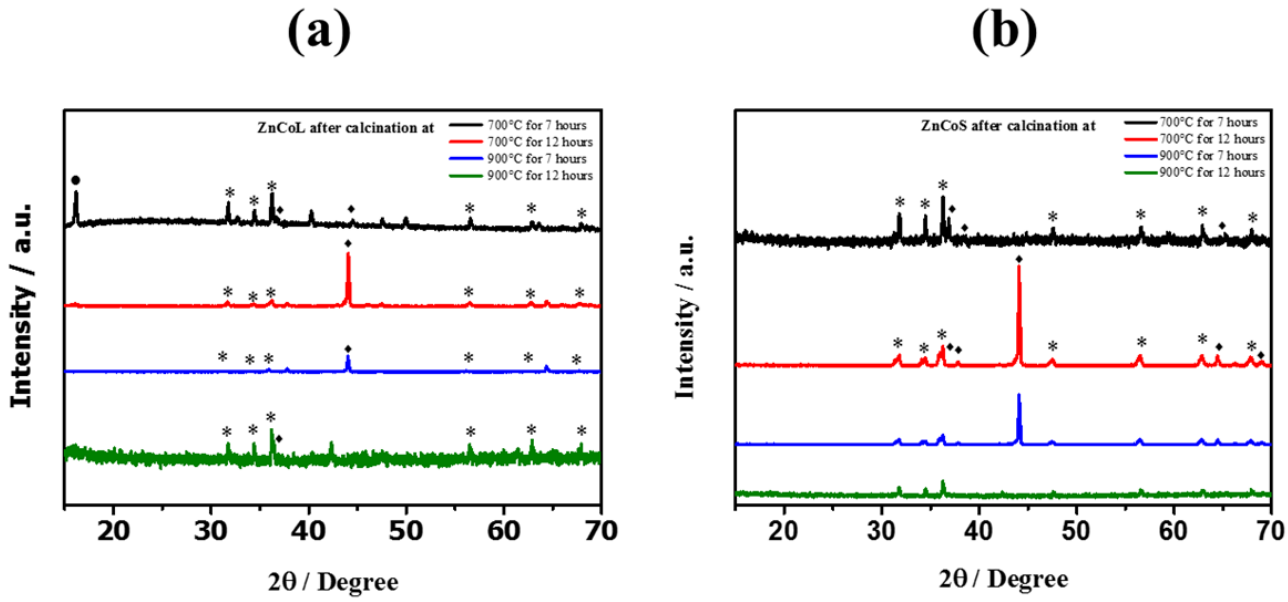

Figure 4. XRPD profile of the products of calcination of ZnCoL (a) at 700 °C - 7 hours (black line); 700 °C - 12 hours (red line); 900 °C - 7 hours (blue line); 900 °C - 12 hours (green line), and ZnCoS (b) at 700 °C - 7 hours (black line); 700 °C - 12 hours (red line); 900 °C - 7 hours (blue line); 900 °C - 12 hours (green line).

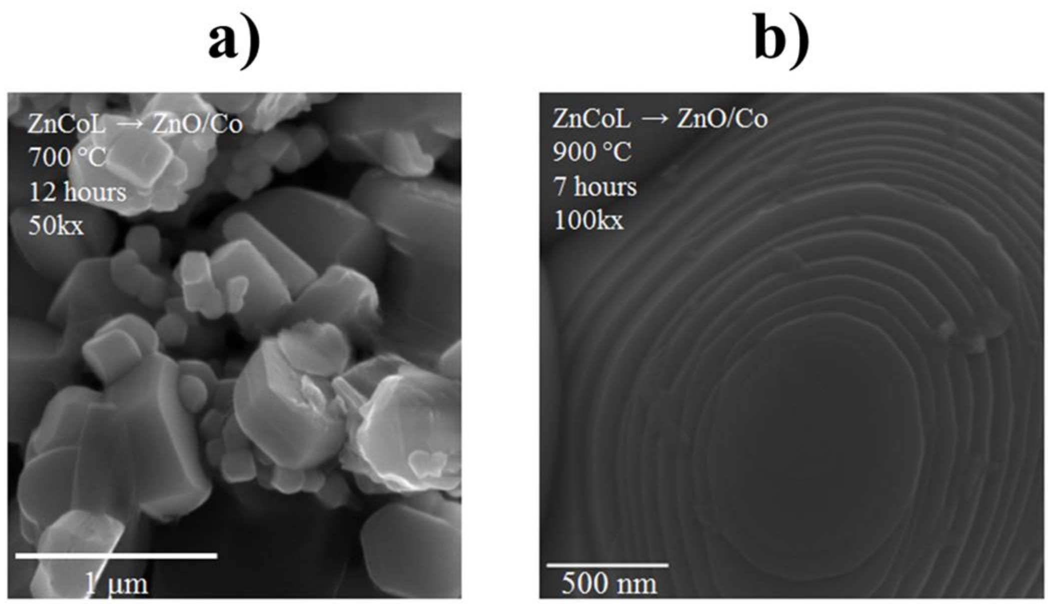

Figure 5. Micrographs of the ZnO/Co from calcination of ZnCoL

reverse micellar phase suffers a great influence on the organic chain present in the structure of the monocarboxylates. Additionally, the size of the stearate groups (18 carbon) in the carboxylate ZnCoS is greater than the size of the laurate groups (12 carbon) in the ZnCoL. This creates more intense intermolecular interactions between the layers to form mesophases [35,36] before the fusion step of each compound during the heat, providing greater protection to the oxide core, avoiding particles coalescence, forming particles with smaller sizes, as can be seen in Figures 7e – 7h [37,38].

3.3 UV-vis Diffuse Reflectance Spectroscopy

Figure 8 illustrates the adjustments of diffuse reflectance in the UV-vis range for ZnO samples doped with cobalt, synthesized by different precursors, calcination temperatures, and times. Table 2 presents the results for direct and indirect band gap adjustments according to the precursor, calcination time, and temperature. Although the values of the indirect band gap are smaller, an additional phonon presence is required, in addition to the photon, for electronic transition in the indirect gap. On the other hand, the direct transition is statistically more feasible, as it only requires the presence of a photon [39].

According to the calcination treatment and precursor, our results indicate that the direct optical gap was approximately 2.4 eV with a variation of 0.2 eV. The literature shows that the optical gap for pure ZnO is around 3.1 eV [40,41]. Alternatively, for CoO the optical gap is less than or equal to 2 eV, depending on the preparation methodology [42,43]. The results show that the cobalt doping reduced the direct optical gap in the samples. These findings are consistent with Kimura *et al.* who sintered samples at 600 and 950 °C for 24 hours in a quartz glass tube [44]. They found that the direct gap of the ZnO-CoO alloy decreases as the CoO content increases and reaches 2.19 eV in the 20 mol% CoO sample.

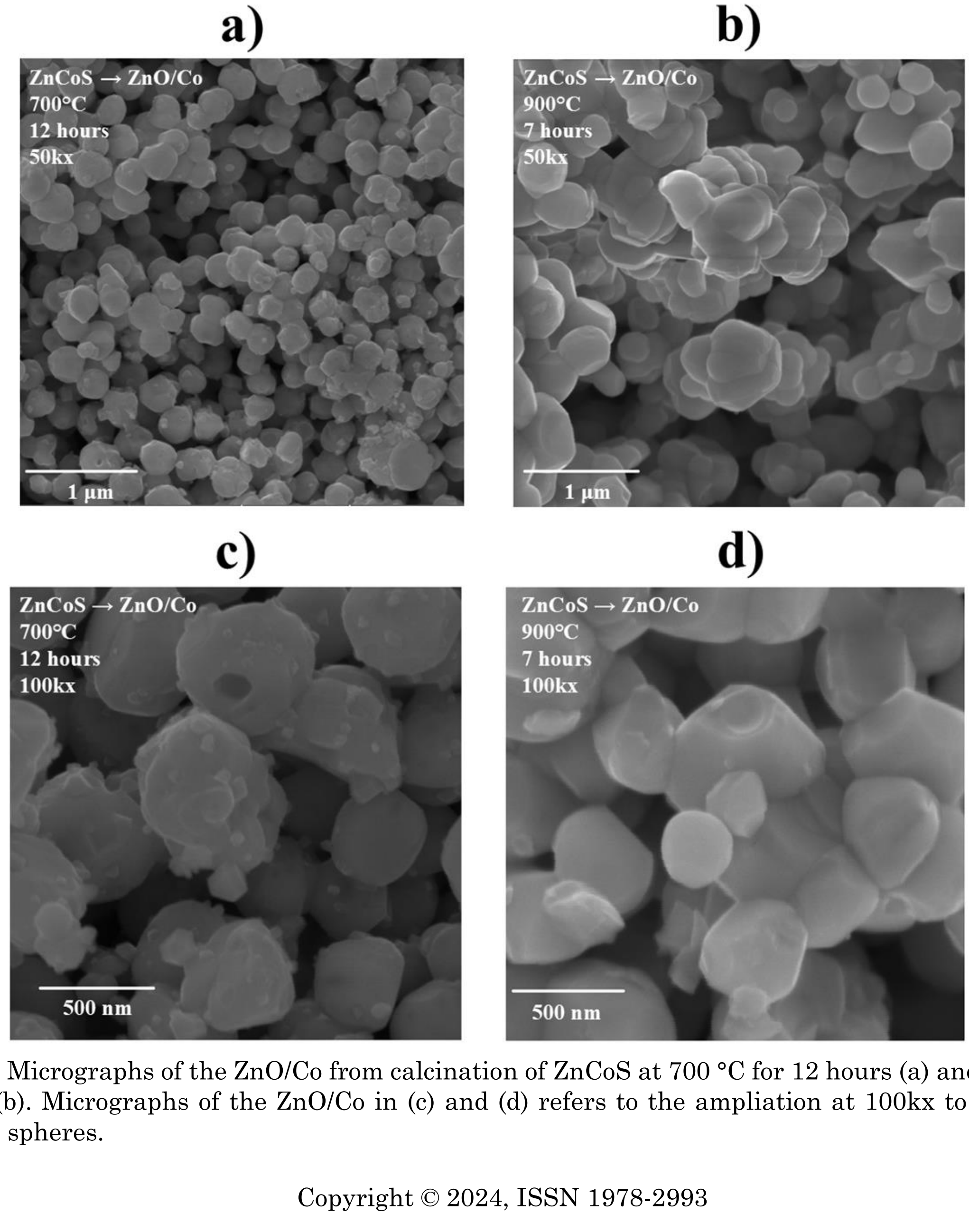

Figure 6. Micrographs of the ZnO/Co from calcination of ZnCoS at 700 °C for 12 hours (a) and 900 °C for 7 hours (b). Micrographs of the ZnO/Co in (c) and (d) refers to the ampliation at 100kx to detach the irregular spheres.

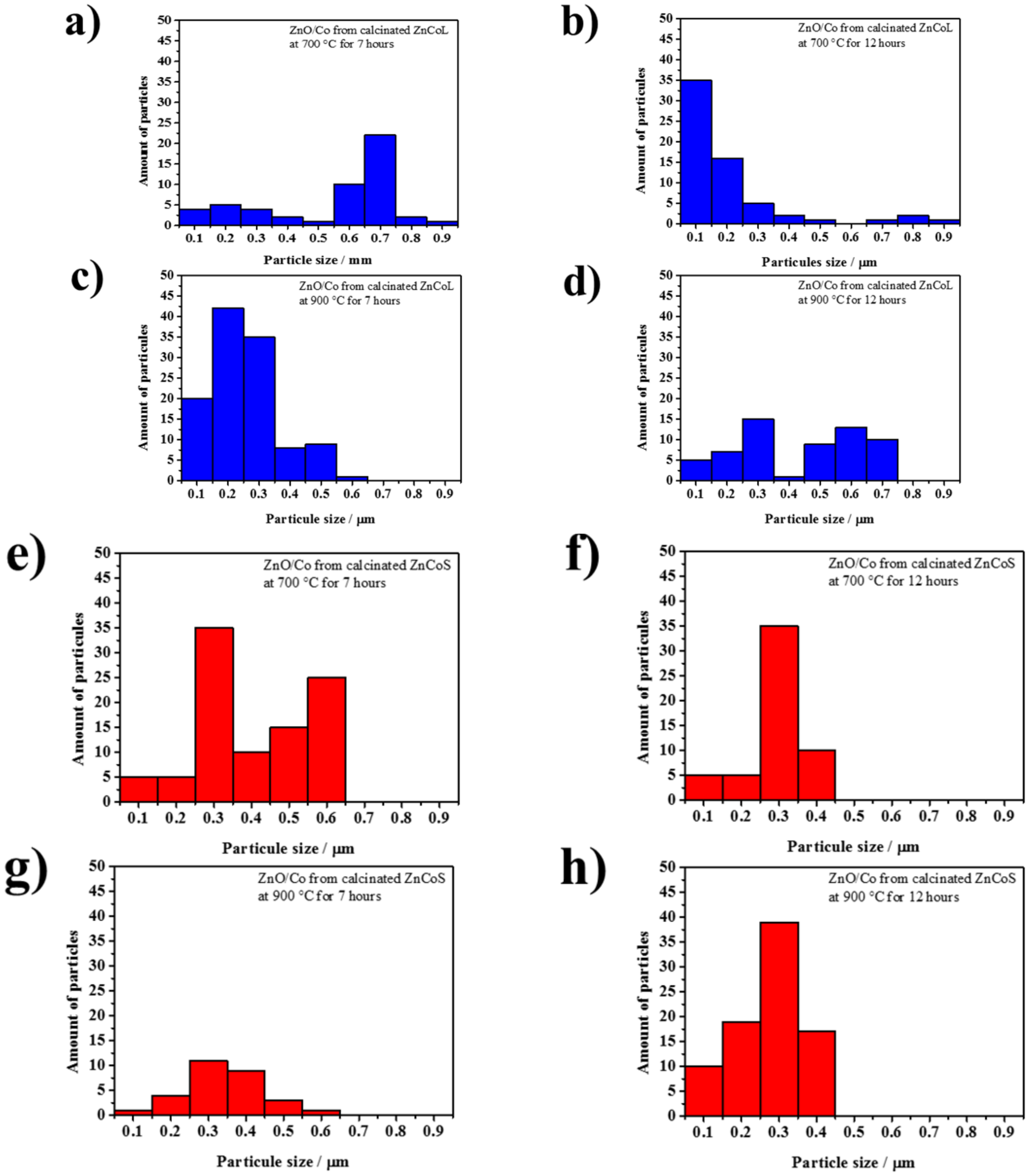

Figure 7. Particle sizes determined for the ZnO/Co obtained from ZnCoL (a – d) and ZnCoS (e – h).

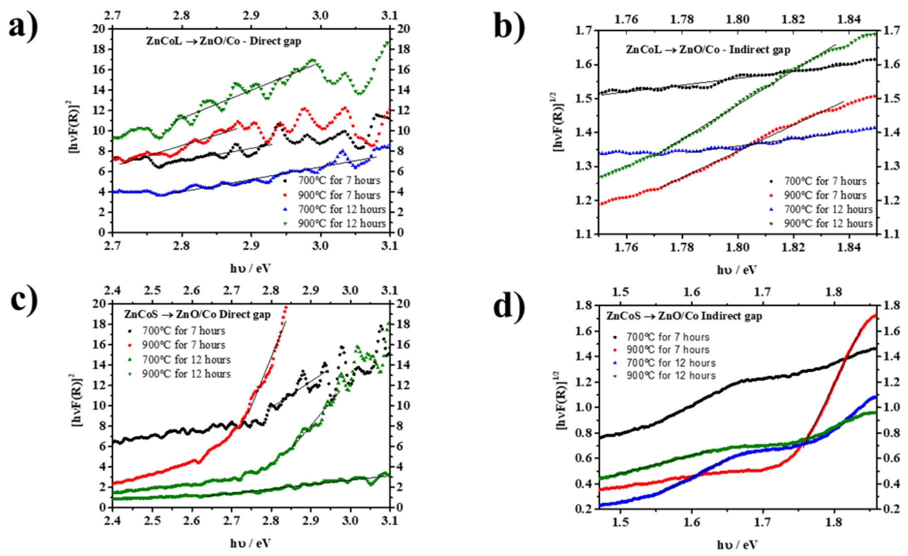

Figure 8. KM Model applied to diffuse reflectance data for samples prepared using precursor (a) ZnCoL for direct band gap, (b) ZnCoL for indirect band gap, (c) ZnCoS for direct band gap, and (d) ZnCoS for indirect band gap. The graphs indicate the number of hours and the sample calcination temperature.

Although there is a significant band-gap variation in the samples with lower CoO content, it becomes smaller in the high-CoO concentration samples. Indeed, the reduction in the optical gap is significant for the photodegradation of chemical contaminants in water, as it allows radiation absorption in the higher-intensity region of the solar spectrum. This, in turn, enables a more efficient photodegradation process for water decontamination.

3.4 Methyl Orange Photodegradation Experiments

The control experiment did not present MO photodegradation (see Supporting Information (SI) S3). However, both synthesized materials presented photodegradation activity on methyl orange under UV-visible light, as can be seen in Figures 9a and 9b. After a first step (30 minutes) with the UV-vis lamp turned off, to exclude any possible adsorption process, the lamp was turned on to initiate the photodegradation of MO (Figure 9c). Despite both oxides being active on MO photodegradation, the curve for the ZnO/Co prepared from the laurate precursor, ZnCoL, showed a kp equal to 0.00185 min^{-1} (Figure 9d), a slower photodegradation process than that observed for the ZnO/Co obtained from the stearate precursor, ZnCoS, which was equal to 0.00860 min^{-1} (Figure 9e). Both values are similar,

Table 2. Parameters obtained through the KM method. The columns indicate the precursors, calcination time and temperature, and the values of direct and indirect band gaps.

Precursor	Time (h)	Temperature (°C)	$E_g(eV)$ direct	$E_g(eV)$ indirect
ZnCoS	7.0	700	2.4±0.2	1.24±0.01
ZnCoS	7.0	900	2.6±0.2	1.70±0.03
ZnCoS	12.0	700	2.7±0.1	1.44±0.01
ZnCoS	12.0	900	2.4±0.1	1.16±0.01
ZnCoL	7.0	700	2.2±0.3	0.25±0.05
ZnCoL	7.0	900	2.4±0.2	1.45±0.03
ZnCoL	12.0	700	2.4±0.1	0.55±0.07
ZnCoL	12.0	900	2.4±0.2	1.51±0.01

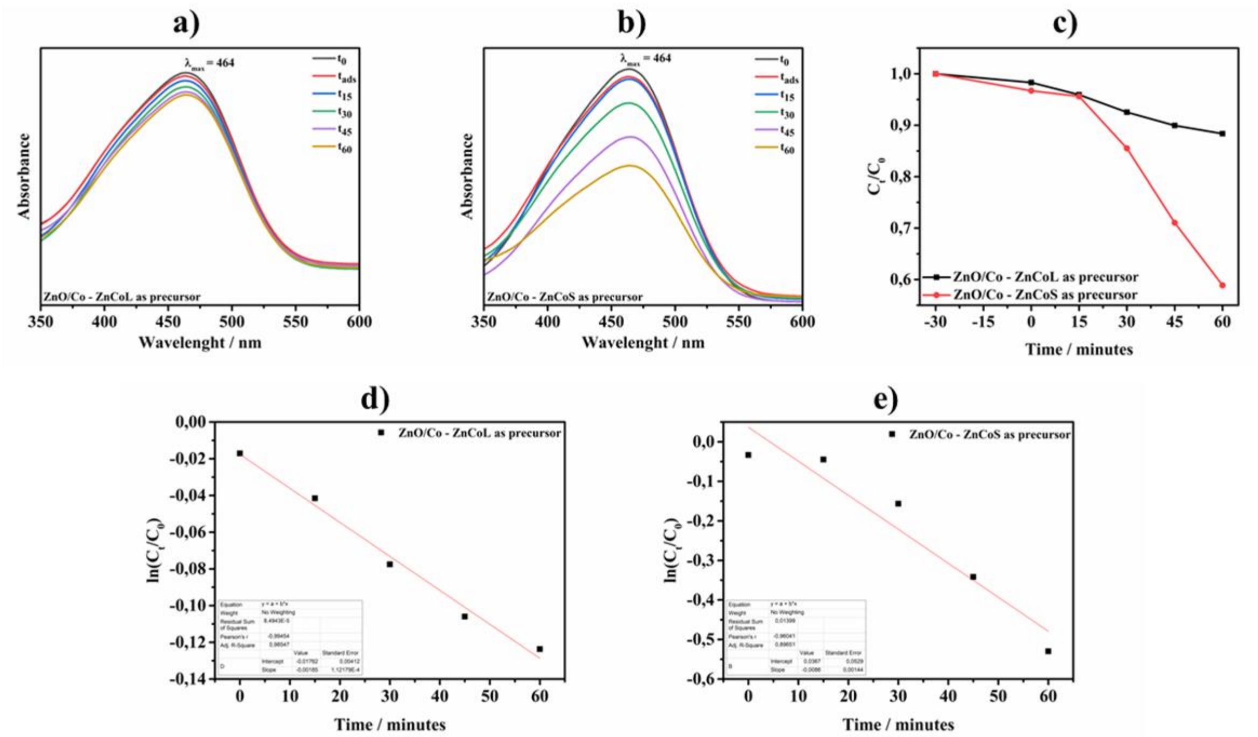

Figure 9. Photodegradation experiments of methyl orange dye. a) UV-Vis absorbance spectra of MO versus time applying the ZnO/Co obtained from ZnCoL as precursor, b) UV-Vis absorbance spectra of MO versus time applying the ZnO/Co obtained from ZnCoS as precursor; c) Ct/C0 curves for MO degradation, black line: ZnO/Co obtained from ZnCoL as precursor and red line: ZnO/Co obtained from ZnCoS as precursor; d and e) ln Ct/C0 versus time (ln $(C_t/C_0) = -k_pt$) of the materials ZnO/Co obtained from ZnCoL and ZnO/Co obtained from ZnCoS, respectively.

but a little faster, than the one obtained by Dey and Das (2020), 0.00323 min^{-1}, using CdS nanocrystals, lower than the obtained for pure ZnO by Kaur and Singhal, which was 0.0573 min^{-1} (under UV light), and very near to those reported by Barick *et al.*, 0.002 min^{-1} for ZnO doped with Co (under UV light) [45-47]. These last authors also reported the decrease in MO photodegradation occurred when they doped the ZnO with Mn^{2+}, Co^{2+}, Ni^{2+}, and Cu^{2+} because the presence of these transition ions promotes the recombination of electrons and holes, resulting in less radical hydroxyl availability for MO degradation [47,48].

Comparing the two materials prepared, the one produced from the ZnCoS showed a faster photodegradation rate than the material generated from the ZnCoL. Considering the band gap obtained for each material (see Table 2), the photocatalytic activity could have values of degradation rate very close for both solids because the direct and the indirect gaps are very similar. Also, the Zn/Co/O ratio and distribution (see Figures S1 and S2) were almost the same for each solid. Therefore, since the morphology of these two ZnO/Co materials were different, prisms-like and sphere-like, the surface activity can lead to the photodegradation rates observed [48-53].

Besides the spherical morphology, the ZnO/Co from ZnCoS calcination also presented the smallest particle sizes (Figure 7). Tripathy *et al.* synthesized porous spherical ZnO with rapid activity in MO photodegradation formed by nanosheets [53]. The surface exposure in spherical morphology can enhance the radical hydroxyl generation (OH•) during the photocatalysis, because this shape favors the interaction between the ZnO/Co particles and UV-visible light, resulting in radical formation and has a more exposed surface, what turns more effective to interact with water molecules that gives origin at the OH• and superoxide, that acts in the dye degradation [52-55]. So, this turns the ZnO/Co originated from ZnCoS more promising than the ZnO/Co obtained from ZnCoL.

4. Conclusions

The zinc oxide doped with cobalt (ZnO/Co) produced by saturated monocarboxylates as precursors (laurate and stearate) presented different morphology and photocatalytic rates on methyl orange photodegradation. The longer carbonic chain from stearate preferred the spherical morphology for particles of ZnO/Co, and consequently, this material had the faster photodegradation rate for MO. The material presented good activity compared to similar solids in the literature, being active under visible light irradiation. Thus, using monocarboxylates as templates for mixed oxide obtention, with application in water treatment for dye removal, is very plausible and leverages the reuse of matrices containing cobalt and monocarboxylate waste.

Acknowledgment

The authors would like to thank the Material Chemical Group (Grupo de Química de Materiais – GQM) from the Federal University of Paraná, Structural Characterization Laboratory (Laboratório de Caracterização Estrutural-LCE) and the Institute of Physics and Chemistry from the Federal University of Itajubá (IFQ-UNIFEI).

CRediT Author Statement

H.I.F. Correa: Conceptualization, Formal analysis, Methodology, Writing – original draft. R.R. Ramalho Jr: Formal analysis and Methodology. A.F. Oliveira: Formal analysis, Methodology, Validation and Writing – review & editing. F.S. Lisboa: Conceptualization, Formal analysis, Methodology, Resources, Supervision, Validation and Writing – review & editing.

Supporting Information (SI)

Energy Dispersive X-Ray (EDX) spectra, elemental mapping, and graphic of methyl orange control experiments are available on Supporting Information, Figures S1, S2 and S3, respectively. Thus, any datasets used during the current study are available from the corresponding author on reasonable request.

References

[1] Kumar, J.A., Krithiga, T., Sathish, S., Renita, A.A., Prabu, D., Lokesh, S., Geetha, R., Namasivayam, S.K.R., Sillanpaa, M. (2022). Persistent organic pollutants in water resources: Fate, occurrence, characterization and risk analysis. *Sci. Total Environ*, 831, 154808. DOI: 10.1016/j.scitotenv.2022.154808.

[2] Hanafi, M.F., Sapawe, N. (2020). A review on the current techniques and technologies of organic pollutants removal from water/wastewater. *Mater. Today: Proc.*, 31, A158–A165. DOI: 10.1016/j.matpr.2021.01.265.

[3] Kaur, J., Bansal, S., Singhal, S. (2013). Photocatalytic degradation of methyl orange using ZnO nanopowders synthesized via thermal decomposition of oxalate precursor method. *Phys. B*, 416, 33–38. DOI: 10.1016/j.physb.2013.02.005.

[4] Peerakiatkhajohn, P., Butburee, T., Sul, J.-H., Thaweesak, S., Yun, J.-H. (2021). Efficient and Rapid Photocatalytic Degradation of Methyl Orange Dye Using Al/ZnO Nanoparticles. *Nanomaterials*, 11, 1059. DOI: 10.3390/nano11041059.

[5] Sha, Y., Mathew, I., Cui, Q., Clay, M., Gao, F., Zhang, X.J., Gu, Z. (2016). Rapid degradation of azo dye methyl orange using hollow cobalt nanoparticles. *Chemosphere*, 144, 1530–1535. DOI: 10.1016/j.chemosphere.2015.10.040.

[6] Rajendran, M., Bhattacharya, A.K. (1999). Low-temperature formation of alpha alumina powders from carboxylate and mixed carboxylate precursors. *Mater. Lett.*, 39, 188–195. DOI: 10.1016/s0167-577x(99)00004-x.

[7] Barman, S., Vasudevan, S. (2006). Melting of Saturated Fatty Acid Zinc Soaps, *J. Phys. Chem. B*, 110, 22407–22414. DOI: 10.1021/jp064306p.

[8] Hermans, J., Keune, K., van Loon, A., Stols-Witlox, M., Corkery, R., Iedema, P. (2014). The synthesis of new types of lead and zinc soaps: a source of information for the study of oil paint degradation. In J. Bridgland (Ed.), Building strong culture through conservation: preprints ICOM-CC 17th Triennial Conference, 1603.

[9] Peultier, J., Rocca, E., Steinmetz, J. (2003). Zinc carboxylating: a new conversion treatment of zinc. *Corros. Sci.,* 45, 1703–1716. DOI: 10.1016/s0010-938x(03)00020-9.

[10] Guo, G., Shi, C., Tao, D., Qian, W., Han, D. (2009). Synthesis of well-dispersed ZnO nanomaterials by directly calcining zinc stearate. *J. Alloys Comp.*, 472, 343–346. DOI: 10.1016/j.jallcom.2008.04.048.

[11] Boehm, A.K., Husmann, S., Besch, M., Janka, O., Presser, V., Gallei, M. (2021). Porous Mixed-Metal Oxide Li-Ion Battery Electrodes by Shear-Induced Co-assembly of Precursors and Tailored Polymer Particles. *ACS Appl. Mater. Interfaces*, 13, 61166–61179. DOI: 10.1021/acsami.1c19027.

[12] Poizot, P., Laruelle, S., Grugeon, S., Dupont, L., Tarascon, J.-M. (2000). Nano-sized transition-metal oxides as negative-electrode materials for lithium-ion batteries. *Nature*, 407, 496–499. DOI: 10.1038/35035045.

[13] Pal, J., Chauhan, P. (2010). Study of physical properties of cobalt oxide (Co_3O_4) nanocrystals. *Mater. Charact.*, 61, 575–579. DOI: 10.1016/j.matchar.2010.02.017.

[14] Saravanan, R., Gupta, V.K., Narayanan, V., Stephen, A. (2013). Comparative study on photocatalytic activity of ZnO prepared by different methods. *J. Mol. Liq.*, 181, 133–141. DOI: 10.1016/j.molliq.2013.02.023.

[15] Sun, X., You, R., Hu, X., Mo, J., Xiong, R., Ji, H., Li, X., Cai, S., Zheng, C., Meng, M. (2015). Calcination system-induced nanocasting synthesis of uniform Co_3O_4 nanoparticles with high surface area and enhanced catalytic performance. *RSC Adv.*, 5, 35524–35534. DOI: 10.1039/c5ra03271g.

[16] Modwi, A., Ghanem, M.A., Al-Mayouf, A.M., Houas, A. (2018). Lowering energy band gap and enhancing photocatalytic properties of Cu/ZnO composite decorated by transition metals. *J. Mol. Struct.*, 1173, 1–6. DOI: 10.1016/j.molstruc.2018.06.082.

[17] Ali, R.N., Naz, H., Li, J., Zhu, X., Liu, P., Xiang, B. (2018). Band gap engineering of transition metal (Ni/Co) codoped in zinc oxide (ZnO) nanoparticles. *J. Alloys Compd.*, 744, 90–95. DOI: 10.1016/j.jallcom.2018.02.072.

[18] Romeiro, F.C., Marinho, J.Z., Lemos, S.C.S., de Moura, A.P., Freire, P.G., da Silva, L.F., Longo, E., Munoz, R.A.A., Lima, R.C. (2015). Rapid synthesis of Co, Ni co-doped ZnO nanoparticles: Optical and electrochemical properties. *J. Solid State Chem.*, 230, 343–349. DOI: 10.1016/j.jssc.2015.07.026.

[19] Lghazi, Y., Bahar, J., Youbi, B., Ait Himi, M., Elhaimer, C., Elouadrhiri, A., Bimaghra, I., Ouknin, M., Majidi. L. (2021). Nucleation/Growth and Optical Proprieties of Co-doped ZnO Electrodeposited on ITO Substrate. *Biointerface Res. Appl. Chem.*, 12, 6776–6787. DOI: 10.33263/briac125.67766787.

[20] Dou, Q., Ng, K.M. (2016). Synthesis of various metal stearates and the corresponding monodisperse metal oxide nanoparticles. *Powder Technol.*, 301, 949–958. DOI: 10.1016/j.powtec.2016.07.037.

[21] Lisboa, F.S., da Gardolinski, J.E.F., Cordeiro, C.S., Wypych, F. (2012). Layered metal laurates as active catalysts in the methyl/ethyl esterification reactions of lauric acid. *J. Braz. Chem. Soc.*, 23, 39–45. DOI: 10.1590/s0103-50532012000100008.

[22] Hermans, J.J., Keune, K., van Loon, A., Corkery, R.W., Iedema, P.D. (2014). The molecular structure of three types of long-chain zinc(II) alkanoates for the study of oil paint degradation. *Polyhedron*, 81, 335–340. DOI: 10.1016/j.poly.2014.06.030.

[23] Toledo, R.P., Huanca, D.R., Oliveira, A.F., dos Santos Filho, S.G., Salcedo, W.J. (2020). Electrical and optical characterizations of erbium doped MPS/PANI heterojunctions. *Appl. Surf. Sci.*, 529, 146994. DOI: 10.1016/j.apsusc.2020.146994.

[24] Azab, A.A., Esmail, S.A., Abdelamksoud, M.K. (2018). Studying the Effect of Cobalt Doping on Optical and Magnetic Properties of Zinc Oxide Nanoparticles. *Silicon*, 11, 165–174. DOI: 10.1007/s12633-018-9902-4.

[25] Patel, M., Chavda, A., Mukhopadhyay, I., Kim, J., & Ray, A. (2016). Nanostructured SnS with inherent anisotropic optical properties for high photoactivity. *Nanoscale*, 8(4), 2293–2303. DOI: 10.1039/c5nr06731f

[26] Barman, S., Vasudevan, S. (2005). Contrasting Melting Behavior of Zinc Stearate and Zinc Oleate. *J. Phys. Chem. B*, 110, 651–654. DOI: 10.1021/jp055814m.

[27] Ishioka, T., Maeda, K., Watanabe, I., Kawauchi, S., Harada, M. (2000). Infrared and XAFS study on structure and transition behavior of zinc stearate. *Spectrochim. Acta, Part A*, 56, 1731–1737. DOI: 10.1016/s1386-1425(00)00225-0.

[28] Gönen, M., Balköse, D., İnal, F., Ülkü, S. (2005). Zinc Stearate Production by Precipitation and Fusion Processes. *Ind. Eng. Chem. Res.*, 44, 1627–1633. DOI: 10.1021/ie049398o.

[29] Guo, G., Shi, C., Tao, D., Qian, W., Han, D. (2009). Synthesis of well-dispersed ZnO nanomaterials by directly calcining zinc stearate. *J. Alloys Compd.*, 472, 343–346. DOI: 10.1016/j.jallcom.2008.04.048.

[30] Manjula, N., Chen, T.-W., Chen, S.-M., Lou, B.-S. (2021). Facile synthesis of hexagonal-shaped zinc doped cobalt oxide: Application for electroanalytical determination of antibacterial drug ofloxacin in urine samples. *J. Electroanal. Chem.*, 885, 115101. DOI: 10.1016/j.jelechem.2021.115101.

[31] Yang, H., Zhu, X., Zhu, E., Lou, G., Wu, Y., Lu, Y., Wang, H., Song, J., Tao, Y., Pei, G., Chu, Q., Chen, H., Ma, Z., Song, P., Shen, Z. (2019). Electrochemically Stable Cobalt–Zinc Mixed Oxide/Hydroxide Hierarchical Porous Film Electrode for High-Performance Asymmetric Supercapacitor. *Nanomaterials*, 9, 345. DOI: 10.3390/nano9030345.

[32] Imran, M., Kim, D.H., Al-Masry, W.A., Mahmood, A., Hassan, A., Haider, S., Ramay, S.M. (2013). Manganese-, cobalt-, and zinc-based mixed-oxide spinels as novel catalysts for the chemical recycling of poly(ethylene terephthalate) via glycolysis. *Polym. Degrada. Stab.*, 98, 904–915. DOI: 10.1016/j.polymdegradstab.2013.01.007.

[33] Ganguly, A., Kundu, R., Ramanujachary, K.V., Lofland, S.E., Das, D., Vasanthacharya, N.Y., Ahmad, T., Ganguli, A.K. (2008). Role of carboxylate ion and metal oxidation state on the morphology and magnetic properties of nanostructured metal carboxylates and their decomposition products. *J. Chem. Sci.*, 120, 521–528. DOI: 10.1007/s12039-008-0081-5.

[34] Rosenlehner, K., Schade, B., Böttcher, C., Jäger, C.M., Clark, T., Heinemann, F.W., Hirsch, A. (2010). Sodium Effect on Self-Organization of Amphiphilic Carboxylates: Formation of Structured Micelles and Superlattices. *Chem. – Eur. J.*, 16, 9544–9554. DOI: 10.1002/chem.201001150.

[35] Li, H., Bu, W., Qi, W., Wu, L. (2005). Self-Assembled Multibilayers of Europium Alkanoates: Structure, Photophysics, and Mesomorphic Behavior. *J. Phys. Chem. B*, 109, 21669–21676. DOI: 10.1021/jp053980o.

[36] Binnemans, K., Jongen, L., Görller-Walrand, C., D'Olieslager, W., Hinz, D., Meyer, G. (2000). Lanthanide(III) Dodecanoates: Structure, Thermal Behaviour, and Ion-Size Effects on the Mesomorphism. *Eur. J. Inorg. Chem.*, 2000, 1429–1436. DOI: 10.1002/1099-0682(200007)2000:7<1429::aid-ejic1429>3.0.co;2-9.

[37] Tancredi, P., Veiga, L.S., Garate, O., Ybarra, G. (2019). Magnetophoretic mobility of iron oxide nanoparticles stabilized by small carboxylate ligands. *Colloids Surf., A*, 579, 123664. DOI: 10.1016/j.colsurfa.2019.123664.

[38] Neouze, M.-A., Schubert, U. (2008). Surface Modification and Functionalization of Metal and Metal Oxide Nanoparticles by Organic Ligands. *Monatsh. Chem.*, 139, 183–195. DOI: 10.1007/s00706-007-0775-2.

[39] Yuan, L.-D., Deng, H.-X., Li, S.-S., Wei, S.-H., Luo, J.-W. (2018). Unified theory of direct or indirect band-gap nature of conventional semiconductors. *Phys. Rev. B*, 98. DOI: 10.1103/physrevb.98.245203.

[40] Agarwal, S., Jangir, L.K., Rathore, K.S., Kumar, M., Awasthi, K. (2019). Morphology-dependent structural and optical properties of ZnO nanostructures. *Appl. Phys. A*, 125, DOI: 10.1007/s00339-019-2852-x.

[41] Ekennia, A.C., Uduagwu, D.N., Nwaji, N.N., Oje, O.O., Emma-Uba, C.O., Mgbii, S.I., Olowo, O.J., Nwanji, O.L. (2020). Green Synthesis of Biogenic Zinc Oxide Nanoflower as Dual Agent for Photodegradation of an Organic Dye and Tyrosinase Inhibitor. *J. Inorg. Organomet. Polym.*, 31, 886–897. DOI: 10.1007/s10904-020-01729-w.

[42] Wang, Y., Ge, H.X., Chen, Y.P., Meng, X.Y., Ghanbaja, J., Horwat, D., Pierson, J.F. (2018). Wurtzite CoO: a direct band gap oxide suitable for a photovoltaic absorber. *Chem. Commun.*, 54, 13949–13952. DOI: 10.1039/c8cc06777e.

[43] Jiang, H., Gomez-Abal, R.I., Rinke, P., Scheffler, M. (2010). First-principles modeling of localized d states with the GW@LDA+U approach. *Phys. Rev. B*, 82. DOI: 10.1103/physrevb.82.045108.

[44] Akitsugu Kimura, A.K., Yasuhiro Ohbuchi, Y.O., Toshio Kawahara, T.K., Yoichi Okamoto, Y.O., Jun Morimoto, J.M. (2001). Photoacoustic Spectra of ZnO-CoO Alloy Semiconductors. *Jpn. J. Appl. Phys.*, 40, 3614. DOI: 10.1143/jjap.40.3614.

[45] Dey, P.Ch., Das, R. (2020). Enhanced photocatalytic degradation of methyl orange dye on interaction with synthesized ligand free CdS nanocrystals under visible light illumination. *Spectrochim. Acta, Part A*, 231, 118122. DOI: 10.1016/j.saa.2020.118122.

[46] Kaur, J., Singhal, S. (2014). Facile synthesis of ZnO and transition metal doped ZnO nanoparticles for the photocatalytic degradation of Methyl Orange. *Ceram. Int.*, 40, 7417–7424. DOI: 10.1016/j.ceramint.2013.12.088.

[47] Barick, K.C., Singh, S., Aslam, M., Bahadur, D. (2010). Porosity and photocatalytic studies of transition metal doped ZnO nanoclusters. *Microporous and Mesoporous Mater*ials, 134, 195–202. DOI: 10.1016/j.micromeso.2010.05.026.

[48] Ali, A.M., Emanuelsson, E.A.C., Patterson, D.A. (2010). Photocatalysis with nanostructured zinc oxide thin films: The relationship between morphology and photocatalytic activity under oxygen limited and oxygen rich conditions and evidence for a Mars Van Krevelen mechanism. *Appl. Catal. B*, 97, 168–181. DOI: 10.1016/j.apcatb.2010.03.037.

[49] Khan, R., Hassan, M.S., Cho, H.-S., Polyakov, A.Y., Khil, M.-S., Lee, I.-H. (2014). Facile low-temperature synthesis of ZnO nanopyramid and its application to photocatalytic degradation of methyl orange dye under UV irradiation. *Mater. Lett.*, 133, 224–227. DOI: 10.1016/j.matlet.2014.07.006.

[50] Tripathy, N., Ahmad, R., Eun Song, J., Ah Ko, H., Hahn, Y.-B., Khang, G. (2014). Photocatalytic degradation of methyl orange dye by ZnO nanoneedle under UV irradiation. *Mater. Lett.*, 136, 171–174. DOI: 10.1016/j.matlet.2014.08.064.

[51] Tuc Altaf, C., Colak, T.O., Rostas, A.M., Popa, A., Toloman, D., Suciu, M., Demirci Sankir, N., Sankir, M. (2023). Impact on the Photocatalytic Dye Degradation of Morphology and Annealing-Induced Defects in Zinc Oxide Nanostructures. *ACS Omega*, 8, 14952–14964. DOI: 10.1021/acsomega.2c07412.

[52] Gong, J. Lv, W., Huang, K., Zhu, J., Meng, F., Song, X., Sun, Z. (2011). Effect of annealing temperature on photocatalytic activity of ZnO thin films prepared by sol–gel method. *Superlattices Microstruct.*, 50, 98–106. DOI: 10.1016/j.spmi.2011.05.003.

[53] Tripathy, N., Ahmad, R., Kuk, H., Lee, D.H., Hahn, Y.-B., Khang, G. (2016). Rapid methyl orange degradation using porous ZnO spheres photocatalyst. *J. Photochem. Photobiol. B*, 161, 312–317. DOI: 10.1016/j.jphotobiol.2016.06.003.

[54] Sun, Y., Chen, L., Bao, Y., Zhang, Y., Wang, J., Fu, M., … Ye, D. (2016). The applications of morphology controlled ZnO in catalysis. *Catalysts (Basel, Switzerland)*, *6*(12), 188. DOI: 10.3390/catal6120188

[55] Yu, C., Yang, K., Xie, Y., Fan, Q., Yu, J. C., Shu, Q., & Wang, C. (2013). Novel hollow Pt-ZnO nanocomposite microspheres with hierarchical structure and enhanced photocatalytic activity and stability. *Nanoscale*, *5*(5), 2142–2151. DOI: 10.1039/c2nr33595f